Enthalpy of Mixing and Liquid Structure for Mixtures of Primary and Secondary Alcohols: Molecular Simulations and COSMO-SAC Calculations

Chun-Kai Chang [,] and J. Ilja Siepmann [,]

E-mail: siepmann@umn.edu

Abstract

The enthalpy of mixing provides information on the favorability of cross-interactions between two different chemical compounds, and it can be included in the training of activity coefficient models to capture the temperature dependence. Recently, Mathias highlighted that certain mixtures of primary and secondary alcohols exhibit exothermic mixing behavior, whereas mixtures of primary alcohols show the more common endothermic mixing behavior [*Ind. Eng. Chem. Res.* **2019**, *58*, 12465]. Here, we probe the mixing behavior of short-chain alcohols at $T = 298.15$ K and $p = 1$ bar through molecular simulations with the TraPPE–UA force field and molecular modeling with the COSMO-SAC activity coefficient model. Using their predictive modes (i.e., without tuning of the models), neither of these two computational approaches

yields the exothermic mixing behavior for primary and secondary alcohols. To capture the exothermic mixing, we explore modifications of the TraPPE–UA force-field parameters to make the secondary CHOH group a better hydrogen-bond acceptor (through an increase of the partial charge on the oxygen atom), but also adding steric hindrance for hydrogen-bond formation between two secondary alcohols (through an increase of the Lennard-Jones diameter on the α-CH pseudoatom). Detailed analysis of the liquid structures for the neat phases and mixtures indicates that the tuned model yields slightly enhanced cross-association which results in a more significant shift from tetrameric to larger hydrogen-bonded aggregates than for the TraPPE–UA model, whereas neither model exhibits a significant change in the number of hydrogen bonds upon mixing. Thus, the simulations point to a shift from cyclic tetramers and pentamers with strained hydrogen bonds to larger, less strained aggregates as the underlying structural change for the exothermic mixing behavior of primary and secondary alcohols.

Alcohols are widely used chemical compounds in numerous applications, including as solvents, disinfectants, fuel additives, organic modi ers in reversed-phase liquid and supercritical uid chromatography, and industrial feedstock for production of many useful chemicals. Speci cally, methanol (MeOH) as reactant is important for the synthesis of many other common chemicals, such as dimethyl ether, acetic acid, and formaldehyde. Moreover, MeOH can be produced through conversion of CO , leading to a potential product for CO captured from the atmosphere. Propan-2-ol (Pr2OH, often called isopropanol) is commonly used as organic solvent and for cleaning applications. The butanol (BuOH) isomers also nd use as solvents, but are also considered as sustainable biofuels that are completely miscible with gasoline and only moderately hygroscopic, i.e., providing signi cant advantages over ethanol. Because of the wide variety of uses for these short-chain alcohols, accurate

knowledge of their thermophysical properties and phase equilibria is important to understand their function and to design energy-e cient separation processes.

To realize less resource-intensive and economically viable processes, downstream separations, where most valuable chemicals are puri ed, are indispensable. Phase diagrams and associated thermophysical properties are essential to nd operating conditions that minimize the work to separate a mixture. Phase diagrams for mixtures are often constructed by employing thermodynamic (macroscopic) activity coe cient models, also known as (excess Gibbs energy) models, which include NRTL, UNIQUAC, UNIFAC, and COSMO-based models, that utilize knowledge of the phase equilibrium properties of the neat compounds as input. Molecular modeling, particular the various variants of the statistical associating uid theory (SAFT), is also commonly used for the prediction of phase diagrams. Besides thermodynamic and molecular modeling approaches, molecular simulations also allow for the construction of phase diagrams. Monte Carlo or molecular dynamics simulations involve the computation of ensemble or time averages from phase-space or dynamical trajectories for a system consisting of a relatively large number of molecules (typically ranging from hundreds to thousands of molecules). Molecular simulations are, hence, computationally much more demanding than the other forms of molecular modeling. However, molecular simulations not only provide information on the thermophysical and coexistence properties but also detailed structural information that is essential to understanding the microscopic-level origin for observed trends in the macroscopic behavior.

The enthalpy of mixing is one of the most important thermodynamic properties for chemical process design. This property re ects the temperature dependence of activity coef- cients. Recently, Mathias highlighted the atypical behavior for the MeOH/Pr2OH binary mixture where the mixing process is exothermic while other short-chain alcohol mixtures yield endothermic mixing. This indicates that the activity coe cient increases as temperature increases whereas the slope of the activity coe cient to temperature is usually negative for primary primary alcohols. Besides MeOH/Pr2OH, exothermic mixing is also observed

for the binary mixtures of MeOH with secondary or tertiary BuOH. This uncommon behavior leads one to suspect stronger cross-association and signi cant di erences in the number of hydrogen bonds in a primary secondary alcohol mixture. Mathias also encouraged engineers to include this property when training activity coe cient models to capture their temperature dependence and suggested more studies should be addressed from microscopic viewpoints.

The (excess) enthalpy of mixing (__) can be calculated from molecular simulations via separate simulations for the (real) mixture (__) and the neat phases for each of the components that are used to compute the internal energy (or only the potential energy because the kinetic term cancels) and pressure volume term. The enthalpy of mixing is the di erence of enthalpy between the real mixture and the corresponding ideal mixture state as follows:

$$\_\_ = \_\_ \qquad \_\_ \tag{1}$$

where __ is the molar enthalpy of pure component , and is the mole fraction of component in the mixture. For simple molecular models, it is also possible to followed an alchemical path where one starts with a pure system and morphs increasing number of molecules into the other species. For molecular simulations, calculation of the excess properties is challenging from a statistical viewpoint because it involves the calculation of a small di erence between multiple large numbers. For example, for the alcohol mixtures considered here, __ and __ values are 40 kJ/mol, whereas __ values do not exceed 0.4 kJ/mol.

To obtain the (excess) enthalpy of mixing from models, the excess molar Gibbs free energy of the mixture is computed rst, followed by converting the activity coe cients to the enthalpy of mixing through a Maxwell relation:

$$\_\_ = \frac{\ln}{\_\_} \tag{2}$$

where stands for the activity coe cient of component , and and are the molar gas

constant and the absolute temperature, respectively.

In this study, we explore the mixing of short-chain alcohols via Monte Carlo simulations with the TraPPE UA force eld to understand their unusual behavior at the molecular level. Treating each molecule as a exible particle with the interactions represented my multiple sites, we compute macroscopic properties and analyze the simulation trajectories. In addition to the molecular simulations, we utilize the COSMO-SAC activity coe cient model, an implicit solvation/activity coe cient model based on electronic structure calculations, which can also account for directional hydrogen-bonding interactions. We nd that these two approaches with standard parameterization predict endothermic mixing for primary secondary alcohol binary mixtures, which qualitatively disagrees with experimental measurements. Thus, starting from the TraPPE UA model, we develop a molecular model to reproduce the exothermic mixing behavior by increasing the magnitude of the partial charges on the oxygen atom and the CH pseudoatom and also the Lennard-Jones diameter of the CH pseudoatom used to represent the secondary alcohols. These modi cation allow for stronger cross-association with primary alcohols, while increasing the steric penalty for self-association of the secondary alcohols. The structural di erences in mixing of primary primary and primary secondary alcohols are analyzed using radial distribution functions (RDF), number integrals (NI), local composition enhancements (LCE), and cluster size distributions (CSD). The compounds and models used for this study are described in Table 1.

Table 1: Names of Chemical Compounds and Models[a]

name (abbreviation)	linear formula	CAS number	models
methanol (MeOH)	CH OH	67-56-1	T, C
propan-1-ol (Pr1OH)	CH (CH) OH	71-23-8	T, C
propan-2-ol (Pr2OH)	CH CH(OH)CH	67-63-0	T, C, M1, M2, M3, M4, M5
butan-1-ol (Bu1OH)	CH (CH) OH	71-36-3	T, C
butan-2-ol (Bu2OH)	CH CH(OH)CH CH	78-92-2	T, C, M3, M4, M5

[a] T, C, and M denote the TraPPE UA force eld, the COSMO-SAC model, and the modi ed models developed in this study, respectively. All chemical compounds are pure, as speci ed by their corresponding input les.

The TraPPE UA alcohol model treats CH (= 1 2 3) groups as pseudoatoms (or united atoms) with interaction sites at the C atom positions, whereas the O and H atoms of the hydroxyl group are represented by separate interaction sites. The nonbonded interactions between sites and ( ) are represented as follows:

$$= 4 \quad \text{—} \quad \text{—} \quad + \frac{\quad}{4} \tag{3}$$

where , , and are the Lennard Jones (LJ) 12-6 well depth and diameter and the distance between sites and ; and are the partial charge on the -th interaction site and the relative permitivity of vacuum. The nonbonded interactions are calculated for all intermolecular interactions and intramolecular interactions only when sites are separated by four or more bonds (i.e., in this study only for the O atom and the CH pseudoatom in Bu1OH). For the TraPPE UA model, the cross-interaction parameters for unlike interaction sites are obtained using the Lorentz Berthelot combination rules:

$$= \frac{1}{2} \quad + \quad \text{and} \quad = \frac{\quad}{\quad} \tag{4}$$

To account for di erent conformations of the molecules, the TraPPE UA model utilizes angle bending and torsional potentials, whereas the bond lengths are held xed. The bending interactions (also known as 1 3 interactions) are described by harmonic potentials:

$$= \frac{}{2}(\quad) \tag{5}$$

where is the force constant and is the equilibrium bond angle. The torsional motion of sites separated by three bonds (also known as 1 4 interactions) is governed by a cosine

series:

$$= \quad + \quad [1 + \cos \quad] + \quad [1 \quad \cos(2 \quad)] + \quad [1 + \cos(3 \quad)] \tag{6}$$

where are coe cients and is the dihedral angle. The parameters for the TraPPE UA alcohol models are provided in Table S1 (Supporting Information).

Monte Carlo simulations in the isobaric isothermal ( ) ensemble were carried out to determine the molar enthalpy of mixing and liquid density for the TraPPE UA models and the modi ed models for the secondary alcohols. A system size of 1000 molecules was used for neat MeOH, Pr1OH, Pr2OH, Bu1OH, Bu2OH, and the corresponding methanol-containing binary mixtures at a temperature of 298.15 K and a pressure of 1 bar.

The site site LJ interactions were truncated at a cuto radius of 14 A and analytical tail corrections were applied to compensate for the truncated interactions. The Coulomb interactions were calculated using the Ewald summation technique with the convergence parameter = 3 2 . All MC simulations in this work were performed with the in-house Monte Carlo for Complex Chemical Systems Minnesota (MCCCS MN) software.

For a given system, all molecules are initially placed into a layered structure. Several thousand MC cycles (MCCs, where each cycle consists of = 1000 randomly selected moves) at elevated temperature (around 3000 K) were used to yield a disordered structure, followed by several thousand MCCs to pre-equilibrated the system at the target temperature. During these two stages, only translational, rotational, and coupled-decoupled con gurational-bias Monte Carlo moves were utilized. For the equilibration and production periods, volume moves were added. All systems were equilibrated for 10 MCCs. The production periods for the neat primary alcohols and the primary primary binary mixtures consisted of 10 MCCs. Approximately 20-times longer production periods were used for the neat secondary species with the TraPPE UA model and the M4 model to yield comparable uncertainties with those obtained for neat MeOH for the calculation of the enthalpy of mixing and the change of the number of hydrogen bonds. For all systems, 16 independent simulations were performed. From those, the statistical uncertainties were estimated and reported as the 95% con dence

intervals.

The activity coe cient of component is described by COSMO-SAC ($^{-}$) as the following

$$\ln \quad ^{-} = \ln \quad + \ln \tag{7}$$

where the combinatorial term (comb) takes into account the size and shape e ects of the molecule of interest and the residual term (res) considers the electrostatic e ect. The combinatorial term is described by the Staverman Guggenheim (SG) model

$$\ln \quad = \ln — + 5\_ \ \ln — \quad — \tag{8}$$

with $= (\ \_) \quad \_ ,$ $= (\ \_) \quad \_ ,$ and $= 5(\_ \quad \_) \quad (\_ \quad 1)$ where $\_$ and $\_$ are the normalized volume and the surface area of component , respectively.

The residual term is written as the sum of the di erence between the segment activity coe cient in a solvent ( ) and its neat state ( ):

$$\ln \quad = — \underset{m}{\text{COSMO}} \quad (\quad) \ \ln \quad (\quad) \quad \ln \quad (\quad) \tag{9}$$

where is the surface area of species , and is the e ective contact area between two molecules. The term ( ), denoted as the -pro le , is the ratio of the surface area of segments whose charge density is to .

The segment activity coe cient of a pure component (=) and a mixture (=) can be determined by

$$\ln \quad (\quad) = \ln \underset{n}{\text{COSMO}} \quad (\quad) \quad (\quad) \exp \frac{(\quad)}{} \tag{10}$$

with

$$(\qquad) = \qquad + \frac{}{} \qquad + \qquad + \max\ 0 \qquad \min\ 0 \qquad + \tag{11}$$

where ( ) is the segment interaction of segments and ; and are parameters that describe electrostatic interactions; describes hydrogen bonding interactions; and represent the charge density of a segment or that is associated with a proton acceptor or donor atom, respectively; is a threshold to lter out weak charge density segments that should not contribute to HB interactions (i.e., = = 0 if the segment or is not classi ed as an HB segment). To classify the type of each segment, the directional hydrogen bond (DHB) scheme proposed by Chen and Lin was used along with the determination of the lone pair positions as the hydrogen bond centers of proton acceptors by potential local minima in molecular electrostatic potential (MESP) map proposed by Chang All segments located within the cuto radius, , from a hydrogen bond center were classi ed as or . The parameters utilized in this study are provided in the Supporting Information.

The enthalpy of mixing of the binary mixtures (Eq. 2) were calculated using the COSMO-SAC model with directional hydrogen bonding interactions. The COSMO calculations, which generate -pro les (Fig. S1), followed the same approach as described in prior works. The electronic structure calculations were conducted with the Amsterdam Density Functional (ADF) software using the Becke Perdew functional with the TZP basis set.

The numerical data for molar enthalpies and enthalpies of mixing calculated from the Monte Carlo simulations and COSMO-SAC calculations are reported in Tables 2 and 3. Fig. 1 shows a comparison of the __ values predicted with the COSMO-SAC and TraPPE

Table 2: Molar enthalpy, molar enthalpy of mixing, and the product of pressure and molar volume of mixing obtained from Monte Carlo simulations for binary mixtures of short-chain alcohols at = 298 15 K and = 1 bar. The labels T and M4 in parenthesis denote compounds represented with the TraPPE UA model and the modified M4 model, respectively. Uncertainties ( ) are reported as 95% confidence intervals.

MeOH	—	—	— mix	— mix	— mix	— mix	—	—	— mix	— mix	— mix	— mix
	−						−					
	−						−					
	−						−					
	−						−					
	−						−					
	−						−					
	−						−					
	−						−					
	−						−					
	−						−					
	−						−					
	−						−					
	−				−		−					
	−						−					
	−						−					
	−						−					
	−						−					
	−						−					
	−						−					
	−						−					
	−						−					
	−						−					
	−						−					
	−		−		−		−		−			
	−		−		−		−		−		−	
	−		−		−		−		−		−	
	−		−		−		−		−		−	
	−		−		−		−		−		−	
	−		−		−		−		−		−	
	−		−		−		−		−		−	
	−		−		−		−		−		−	
	−		−		−		−		−		−	
	−						−					

UA models and obtained from experimental measurements for the MeOH/Pr1OH and MeOH/Bu1OH mixtures. Both models correctly predict the endothermic mixing behavior for these primary primary alcohol mixtures. For the MeOH/Pr1OH mixture, both models predict a nearly symmetric curve with a maximum for — at = 0 5, and a very slight tilt to higher 0 55 for the MeOH/Bu1OH mixture. The experimental data indicate a more asymmetric behavior with the maxima located at 0 58 and 0 62 for the MeOH/Pr1OH and MeOH/Bu1OH mixtures, respectively. The TraPPE UA model

Table 3: Molar enthalpy mixing from COSMO-SAC calculations for binary mixtures of short-chain alcohols at = 298 15 K.

x_1	γ_1	γ_2	$\frac{\partial \ln \gamma_1}{\partial T}$ /K^{-1}	$\frac{\partial \ln \gamma_2}{\partial T}$ /K^{-1}	$\Delta \underline{H}^{\mathrm{mix}}$ /(kJ/mol)	γ_1	γ_2	$\frac{\partial \ln \gamma_1}{\partial T}$ /K^{-1}	$\frac{\partial \ln \gamma_2}{\partial T}$ /K^{-1}	$\Delta \underline{H}^{\mathrm{mix}}$ /(kJ/mol)
MeOH (1)/Pr1OH (2)						MeOH (1)/Pr2OH (2)				
0.00	1.084	1.000	0.00024	0.00000	0.000	1.068	1.000	0.00014	0.00000	0.000
0.10	1.074	1.001	0.00021	0.00000	0.017	1.061	1.000	0.00013	0.00000	0.010
0.20	1.064	1.002	0.00018	0.00001	0.031	1.054	1.002	0.00011	0.00000	0.019
0.30	1.053	1.006	0.00015	0.00002	0.043	1.046	1.004	0.00010	0.00001	0.026
0.40	1.043	1.011	0.00012	0.00003	0.051	1.037	1.009	0.00008	0.00002	0.032
0.50	1.033	1.019	0.00009	0.00006	0.056	1.029	1.016	0.00006	0.00003	0.035
0.60	1.023	1.031	0.00006	0.00009	0.056	1.020	1.026	0.00005	0.00006	0.036
0.70	1.014	1.048	0.00004	0.00014	0.051	1.013	1.040	0.00003	0.00009	0.034
0.80	1.007	1.070	0.00002	0.00020	0.041	1.006	1.061	0.00001	0.00013	0.027
0.90	1.002	1.102	0.00000	0.00028	0.024	1.002	1.089	0.00000	0.00019	0.016
1.00	1.000	1.145	0.00000	0.00038	0.000	1.000	1.127	0.00000	0.00026	0.000
MeOH (1)/Bu1OH (2)						MeOH (1)/Bu2OH (2)				
0.00	1.126	1.000	0.00065	0.00000	0.000	1.232	1.000	0.00054	0.00000	0.000
0.10	1.114	1.001	0.00057	0.00000	0.045	1.199	1.001	0.00047	0.00000	0.037
0.20	1.100	1.003	0.00050	0.00002	0.084	1.167	1.006	0.00039	0.00002	0.068
0.30	1.085	1.007	0.00042	0.00005	0.115	1.136	1.015	0.00032	0.00004	0.092
0.40	1.070	1.015	0.00033	0.00009	0.138	1.107	1.030	0.00025	0.00008	0.109
0.50	1.055	1.027	0.00025	0.00015	0.151	1.080	1.051	0.00019	0.00013	0.118
0.60	1.040	1.045	0.00018	0.00025	0.152	1.056	1.081	0.00012	0.00021	0.117
0.70	1.026	1.073	0.00011	0.00038	0.140	1.034	1.123	0.00007	0.00030	0.105
0.80	1.013	1.113	0.00005	0.00055	0.112	1.017	1.183	0.00003	0.00043	0.082
0.90	1.004	1.174	0.00001	0.00077	0.066	1.005	1.267	0.00001	0.00057	0.047
1.00	1.000	1.265	0.00000	0.00105	0.000	1.000	1.389	0.00000	0.00070	0.000

over predicts the maximum in __ by factors of 1.8 and 1.5 for the MeOH/Pr1OH and MeOH/Bu1OH mixtures, respectively. In contrast, the COSMO-SAC model under predicts __ for the MeOH/Pr1OH mixture by a factor of 3, but it is spot on for the MeOH/Bu1OH mixture.

Although the experimental data show that the primary secondary alcohol mixtures exhibit exothermic mixing behavior (Fig. 2), the COSMO-SAC and TraPPE UA models predict endothermic mixing as for the primary primary mixtures. The COSMO-SAC model yields rather similar __ values (Table 3) at = 0 5 for the mixtures with the PrOH isomers (0.056 and 0.035 kJ/mol for Pr1OH and Pr2OH, respectively) and the mixtures with the BuOH isomers (0.151 and 0.118 kJ/mol for Bu1OH and Bu2OH, respectively); that is, the COSMO-SAC approach distinguishes mostly with regard to number of carbon atoms

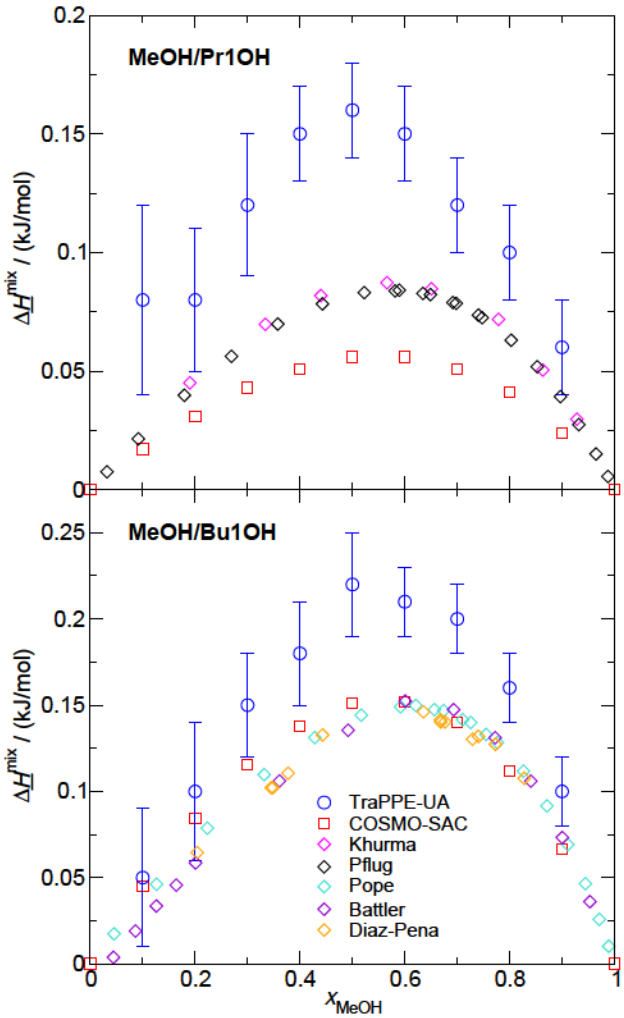

Figure 1: Comparison of the molar enthalpies of mixing for MeOH/Pr1OH (top) and MeOH/Bu1OH (bottom) binary mixtures at 298.15 K and 1 bar predicted with the COSMO-SAC and TraPPE–UA models and measured experimentally.[46–50]

for the alkyl group based on the non-polar part of the σ-profiles but to a lesser extent with regard to position of the hydroxyl group as one may infer from the similarity of the polar parts of the σ-profiles (Fig. S1). In contrast, the TraPPE–UA models shows an increase in the $\Delta \underline{H}^{\mathrm{mix}}$ values for mixtures with the secondary alcohols compared to those with the primary alcohols, whereas a decrease would at least move in the direction of the exothermic behavior observed experimentally.

To capture the exothermic mixing of primary and secondary alcohols, the strategy must be to increase the strength of the cross-association while leaving the strength of the self-

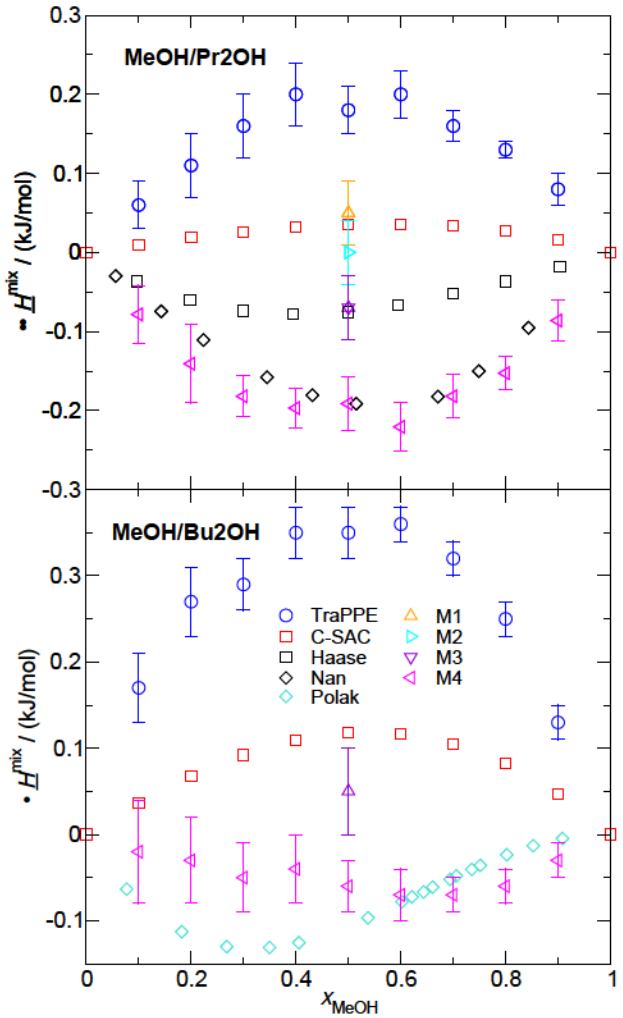

Figure 2: Comparison of the molar enthalpies of mixing for MeOH/Pr2OH (top) and MeOH/Bu2OH (bottom) binary mixtures at 298.15 K and 1 bar predicted with the COSMO-SAC, TraPPE–UA, and modified Mi models and measured experimentally.[29,51,52]

association unchanged to maintain the quality of the predictions of saturated vapor pressure and liquid density for the pure compounds. Of course, one could take the simple route of adding a mixing parameter to the canonical form of the Lorentz-Berthelot combining rules (Eq. 4) to make the Lennard-Jones interactions more favorable, but this ad hoc adjustment would likely fail to capture the underlying reasons for the switch from endothermic to exothermic behavior for primary–primary versus primary–secondary alcohol mixtures. In molecular-mechanics force fields, the strength and steric hindrance for hydrogen bonds of alcohols are controlled by the values of the partial charges and the LJ diameters (if present)

on the hydroxyl H and O atoms and on the CH pseudoatom. Thus, for models that do not place an LJ site at the location of the hydroxyl hydrogen atom, there are six non-bonded interaction parameters (LJ diameter and well depth for the O and CH (pseudo-)atoms and two out of three partial charges on the H, O, and CH (pseudo-)atoms) that could be adjusted while keeping the bonded parameters unchanged. To reduce the parameter space, we consider the choices that were made during the parameterization of the TraPPE UA model for alcohols. In particular, during the parameterization for secondary alcohols, it was observed that transferring the LJ diameter of the CH pseudoatom from 2-methylpropane to Pr2OH, while keeping the other parameters obtained for primary alcohols, leads to an under prediction of the liquid density and over prediction of the saturated vapor pressure, and a choice was made to reduce the LJ diameter for the -CH group in secondary alcohols to 4.33 A from the non-polar CH group value of 4.68 A used in branched alkanes. Here, we explore a di erent path involving an increase in the magnitude of the partial charge on the hydroxyl oxygen atom (and a corresponding increase on the -CH group to maintain neutrality) to strengthen its capability as hydrogen-bond acceptor that is o set by an increase in the LJ diameter for the -CH group leading to enhanced steric hindrance particularly between two secondary alcohols.

As a rst step, we test the e ects of increasing the partial charge on the oxygen atom, , of Pr2OH by 5 and 7.5% while keeping the LJ diameter for the -CH group at 4.33 A (denoted as models M1 and M2, Table 4). The enthalpies of neat Pr2OH and of the equimolar MeOH/Pr2OH mixture are found to decrease linearly with an increase of the absolute value of (Fig. 3, numerical data are provided in Table S3). Encourgingly, the same holds also for the enthalpy of mixing, i.e., the steric hindrance of the secondary alcohol leads to a larger enthalpic e ect for cross-association with methanol than for the self-association of Pr2OH.

Without a compensatory adjustment of the LJ diameter for the -CH group, however, the speci c density of neat Pr2OH is over predicted by 1.0 and 1.4% for models M1 and M2, respectively. As can be seen from the data for liquid densities (Fig. 4; Table S4),

Table 4: Partial charges and LJ diameter for secondary alcohols used here.

	$q_O/\|e\|$	$q_{\alpha C}/\|e\|$	$\sigma_{\alpha C}$/Å
TraPPE–UA[31]	−0.700	+0.265	4.33
M1	−0.735	+0.300	4.33
M2	−0.753	+0.318	4.33
M3	−0.753	+0.318	4.55
M4	−0.770	+0.335	4.55
M5	−0.800	+0.365	4.55

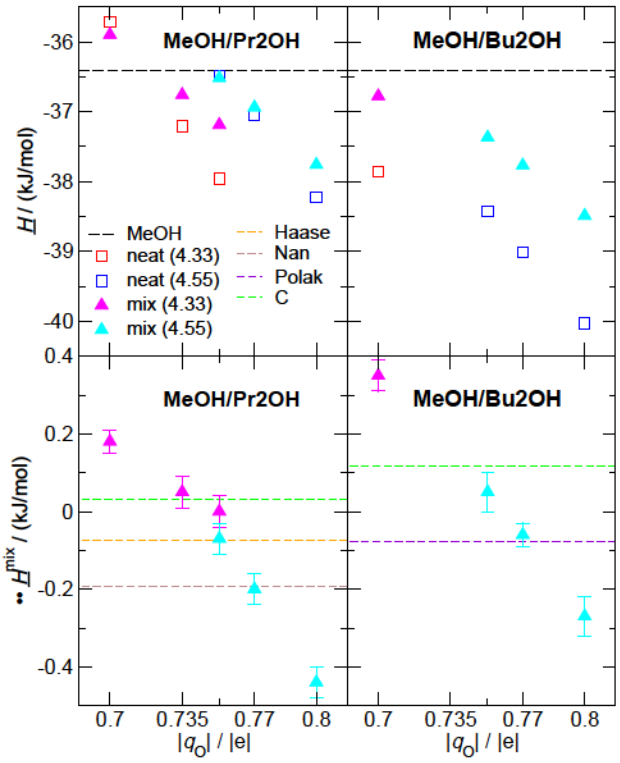

Figure 3: Molar enthalpy (top row) and molar enthalpy of mixing (bottom row) for equimolar MeOH/Pr1OH (left column) and MeOH/Bu2OH (right column) mixtures at 298.15 K and 1 bar as function of the partial charge on the hydroxyl oxygen atom for the secondary alcohols. The $\underline{H}$ for methanol calculated with the TraPPE–UA model and the $\Delta\underline{H}^{\mathrm{mix}}$ values obtained from experiment[29,51,52] and COSMO-SAC calculations are shown as dashed lines. The LJ diameter used for the α-CH group is listed in parenthesis. The uncertainties for $\underline{H}$ values are smaller than the symbol size.

the TraPPE–UA model yields rather accurate predictions for the neat alcohols with the deviations less than 3 kg/m^3 (0.4%); it should be noted that the experimental data reported for neat MeOH in these works ranges from 782 to 787 kg/m^3.[29,53,54] Thus, as a second step,

we increase the LJ diameter for the α-CH group by 5% while keeping $q_O = -0.753$ $|e|$ (model M3). Although an increase of 5% may appear large, the α-CH group of Pr2OH is "buried" by the two methyl groups and the hydroxyl oxygen atom. The liquid density for Pr2OH obtained for model M3 falls 0.6% below the experimental value. As hypothesized, the greater steric hindrance due to the increase in the LJ diameter for the α-CH group also shifts the $\Delta\underline{H}^{\mathrm{mix}}$ value for the equimolar MeOH/Pr2OH into exothermic behavior, and the predicted value agrees quantitatively with the experimental data reported by Haase and Tillmann.[52] However, there is a second experimental data set by Nan *et al.*[51] that indicates a larger magnitude of the exothermic $\Delta\underline{H}^{\mathrm{mix}}$ (Fig. 2).

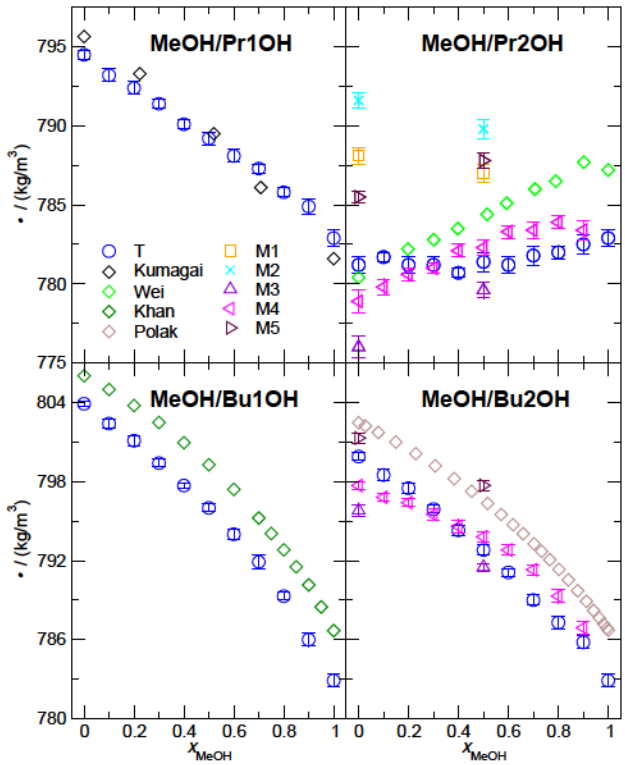

Figure 4: Comparison of the liquid densities for MeOH/Pr1OH (top left), MeOH/Pr2OH (top right), MeOH/Bu1OH (bottom left), and MeOH/Bu2OH (bottom right) mixtures at 298.15 K and 1 bar predicted with the TraPPE–UA and modified Mi models and measured experimentally.[29,53–55] The experimental measurements for MeOH/Bu1OH were conducted at 10 bar.[55]

Thus, as a third step, we test the M3 model for the equimolar MeOH/Bu2OH binary mixtures. Although $\Delta\underline{H}^{\mathrm{mix}}$ is reduced by 0.3 kJ/mol compared to the TraPPE–UA model,

this change is not su cient to cause a switch to exothermic mixing behavior. Furthermore, the liquid density of neat Bu2OH is underestimated by 0.8% for model M3. In response, we test two additional models M4 and M5 that keep = 4 55 A and increase the magnitude of the partial charge on the oxygen atom to 0.770 and 0.800 , repectively (10 and 14% increase, respectively, compared to the TraPPE UA model). Model M4 yields __ for the equimolar MeOH/Pr2OH mixture in excellent agreement with the experimental data by Nan and also very good agreement with the data by Polak for the equimolar MeOH/Bu2OH mixture. The liquid densities for neat Pr2OH and Bu2OH are also satisfactory with under predictions of 0.2 and 0.6%, respectively. Model M5 yields a signi cant over prediction of the magnitude of __ for the equimolar MeOH/Pr2OH and MeOH/Bu2OH mixtures. Thus, model M4 yields the overall best performance for predicting the primary secondary alcohol mixing behavior. Note that simulations also indicate that one of the two con icting experimental data sets for the MeOH/Pr2OH mixture is more consistent with the data for MeOH/Bu2OH, whereas Mathias gives them equal weight.

Before moving on to a detailed structural analysis of the association behavior of the primary primary and primary secondary alcohol mixtures, we compare some other properties for the TraPPE UA and M4 models. Our empirical parameter adjustment indicates that a larger magnitude of the partial charge on the oxygen atom of secondary alcohols is needed to yield exothermic mixing behavior using these molecular mechanics models. Another approach to obtain the value of partial charges relies on quantum mechanical calculations. Table S5 reports the partial charges obtained for the compounds of this study using the charge model 5 (CM5) for isolated molecules in the gas phase with MP2 theory and the 6-311++g(d,p) basis set as implemented in the Gaussian 16 software. The CM5 partial charges are about a factor of 1.4 smaller in magnitude than the e ective partial charges used for the TraPPE UA model, and the quantum-mechanical calculations indicate a small decrease (less than 2%) of the magnitude of for the secondary alcohols compared to their primary isomers, i.e., in the opposite direction than the adjustment made for model M4. The

small variation observed for the CM5 charges is consistent with the -pro les used for the COSMO-SAC calculations (Fig. S1), but the latter model fails to yield the exothermic mixing behavior for the primary-secondary alcohol mixtures. It would be interesting to compute the CM5 charges for dimers representing the binary mixtures studied in this work.

The saturated vapor pressure is an essential property for the design of distillation processes, a proxy for the excess chemical potential of a compound in the liquid phase, and considered in the parameterization of the TraPPE UA force eld. Thus, it is important to check that the adjustments made for model M4 do not yield an unsatisfactory saturated vapor pressure. Rather than construct the entire vapor liquid coexistence curve, the vapor pressure is calculated here only at the experimental normal boiling point of the pure alcohols (see Section S6 for simulation details). Table 5 lists the vapor pressures of the short-chain alcohols at the experimental normal boiling temperature obtained with the TraPPE UA parameters and the modi ed parameters for the M4 model. It is found that the vapor pressures of Pr2OH and Bu2OH using the M4 parameters are underestimated by 10 15% while those obtained with the TraPPE UA model are overestimated by a similar extent with the exception of MeOH for which the saturated vapor pressure is underestimated by 8%. Thus, with regard to vapor pressure at the experimental normal boiling point, the M4 models provides at least comparable accuracy as the TraPPE UA model.

Table 5: Predicted vapor pressures of short-chain alcohols at experimental normal boiling points. The uncertainties ( ) are reported as the 95% con dence interval.

		TraPPE UA		Model M4	
	/K	/kPa	( ) /kPa	/kPa	( ) /kPa
MeOH	338	93	2		
Pr1OH	370	113	2		
Pr2OH	355	115	2	86	3
Bu1OH	391	121	1		
Bu2OH	373	120	2	90	2

Another important quantity for the use of alcohols as solvents is their relative permititivity. The relative permitivity of a compound is correlated with the strength of its molecular

dipole moment but it is also in uenced by the dipole dipole ordering. Thus, we need to check that the increased molecular dipole moment associated with the increase in the partial charges for the M4 model does not result in a relative permitivity out of line with that for the primary alcohols represented by the TraPPE UA model. To this extent, we carried out Monte Carlo simulations in the canonical ensemble (see Section S7 for simulation details). For the primary alcohols, the TraPPE UA model yields relative permitivity values with a ratio of 1:0.52:0.44 for MeOH:Pr1OH:Bu1OH compared to the ratio of 1:0.62:0.53 from experimental measurements (Table 6). The agreement for the relative permitivity ratio for primary alcohols of di erent chain length is satisfactory. The observed decrease in the relative permitivity with increasing chain length for alcohol models with exactly the same molecular dipole moment (set of partial charges, see Table 4) is an illustration of the e ects due to the di erent extent of dipole dipole ordering and clustering (see below) caused by the packing constraints of the non-polar tails. However, the magnitude of the relative permitivities obtained for the TraPPE UA model is about 30% smaller than the experimental values. This is a design feature for non-polarizable force elds that ignore uctuations of the electron clouds and, by default, yield a relative permitivity of unity for non-polar alkanes; i.e., attempting to match the experimental values for the relative permitivities of dipolar molecules would yield to larger deviations for mixtures of polar and non-polar compounds. Turning to the secondary alcohols, we observe that the M4 model does not yield an increase in the relative permitivities compared to the TraPPE UA model. It should also be noted that the relative permitivity values obtained from the Monte Carlo simulations for the TraPPE UA model seem to be somewhat lower than the values previously calculated from molecular dynamics simulations, but the statistical uncertainties of the Monte Carlo simulations are relatively large illustrating that aggregation of alcohols (see below) leads to challenges for the sampling e ciency of Monte Carlo simulations relying on rotational moves for individual molecules.

We also examined whether there may be a need to reparametrize the bonded torsion

Table 6: Relative permitivity (of alcohols examined in this study calculated via Monte Carlo simulations for the TraPPE UA and the M4 models at = 293 15 K compared to molecular dynamics (MD) data for the TraPPE UA model and experimental data. The uncertainties ( ) for the MC simulations are reported as the 95% con dence intervals.

	TraPPE UA		Model M4		MD	Expt.
		( )		( )		
MeOH	25	2				33.3
Pr1OH	13	2			15.2	20.8
Pr2OH	13	1	13	2	14.2	20.2
Bu1OH	11	2				17.8
Bu2OH	9	2	9	3	11.1	17.3

parameters for the CH CH O H angle in the secondary alcohols. Figure S2 shows the CH CH O H dihedral angle distributions for Pr2OH molecules in their pure liquid form and in the equimolar mixture with MeOH obtained from simulations using the TraPPE UA and M4 models. There are minor di erences in the peak heights between the pure liquid and the equimolar mixture, but no di erence is observed between the TraPPE UA and M4 models. Thus, the dihedral distribution does not appear to re ect a di erence for models that capture or fail to capure the exothermic mixing behavior.

Exothermic mixing behavior is often taken as a sign for preferential aggregation of unlike species, whereas endothermic mixing behavior is taken as a sign for partial demixing due to more favorable interactions of the like species. To provide a visual impression of the mixing behavior, snapshots of the MeOH/(primary or secondary PrOH or BuOH) mixtures are depicted in Fig. 5 in a manner that highlights clusters of hydroxyl oxygen atoms using di erent colors for MeOH (red) and the C3/C4 alcohols (green). Our eyes can decipher that the volume fraction of polar groups is smaller for the MeOH/BuOH mixtures (Fig. 5(d)-(f)) than for the MeOH/PrOH mixtures (Fig. 5(a)-(c)). However, there is no obvious di erence between mixtures containing primary versus secondary PrOH or BuOH alcohols nor between systems showing endothermic versus exothermix mixing behavior. Thus, the

structural di erences are rather subtle, and quantitative metrics need to be employed.

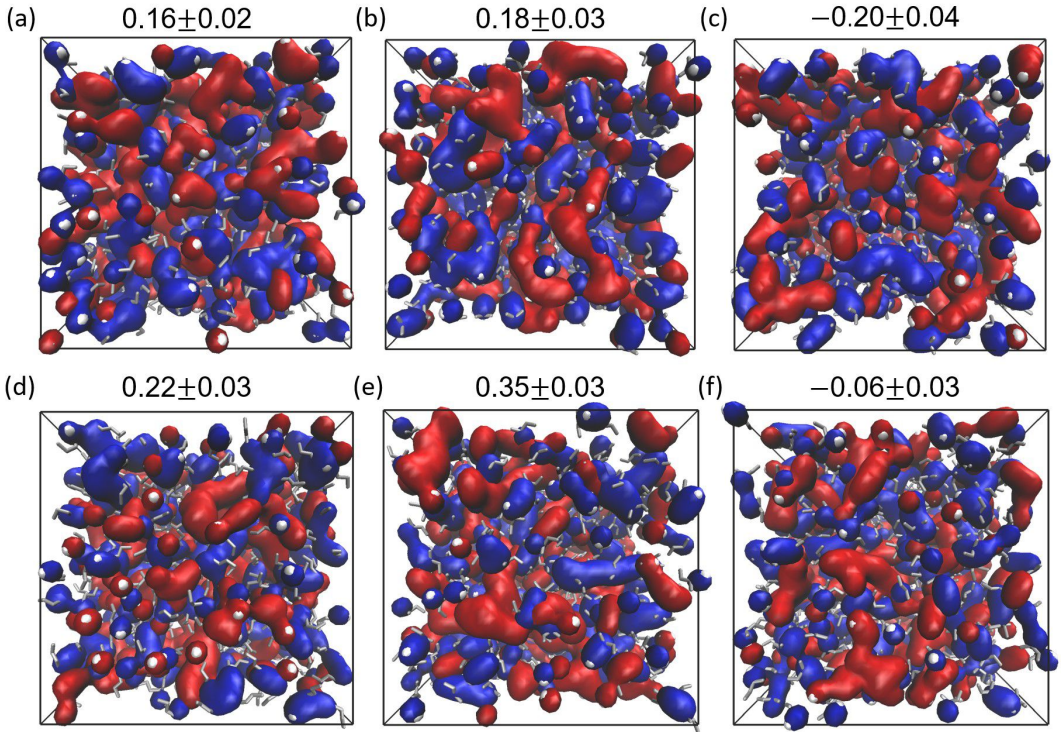

Figure 5: Snapshots of equimolar mixtures of MeOH and PrOH isomers (a, b, and c) and MeOH and BuOH isomers (d, e, and f) at 298.15 K and 1 bar: (a and c) mixtures of MeOH and the primary alcohols: (b and e) MeOH and the secondary alcohols using the TraPPE UA model; (c and f) MeOH and the secondary alcohols using the M4 model. The number on top of each snapshot gives the molar enthalpy of mixing in kJ/mol. The red and blue blobs represent regions populated by oxygen atoms belonging to MeOH and (PrOH or BuOH) molecules, respectively, where the regions are determined with the Quicksurf function in VMD. The gray sticks and white balls represent alkyl tails and hydroxyl hydrogen atoms, respectively.

The oxygen oxygen (O O) radial distribution functions (RDFs) and the corresponding number integrals (NIs) for the mixtures of methanol with Pr2OH and Bu2OH are shown in Fig. 6. The rst peak, indicative of hydrogen-bonded pairs of molecules, occurs at 2.8 A for all systems. That is, increasing the LJ diameter for the -CH pseudoatoom from 3.75 A for MeOH to 4.33 A for secondardy alcohols represented by the TraPPE UA model to 4.55 A for the M4 model does not yield to an outward shift of the hydrogen bond distance. Apparently, this distance is predominantly controlled by the common LJ diameter for the hydroxyl oxygem atom with its nine times larger LJ well depth than that for the CH pseudoatom of

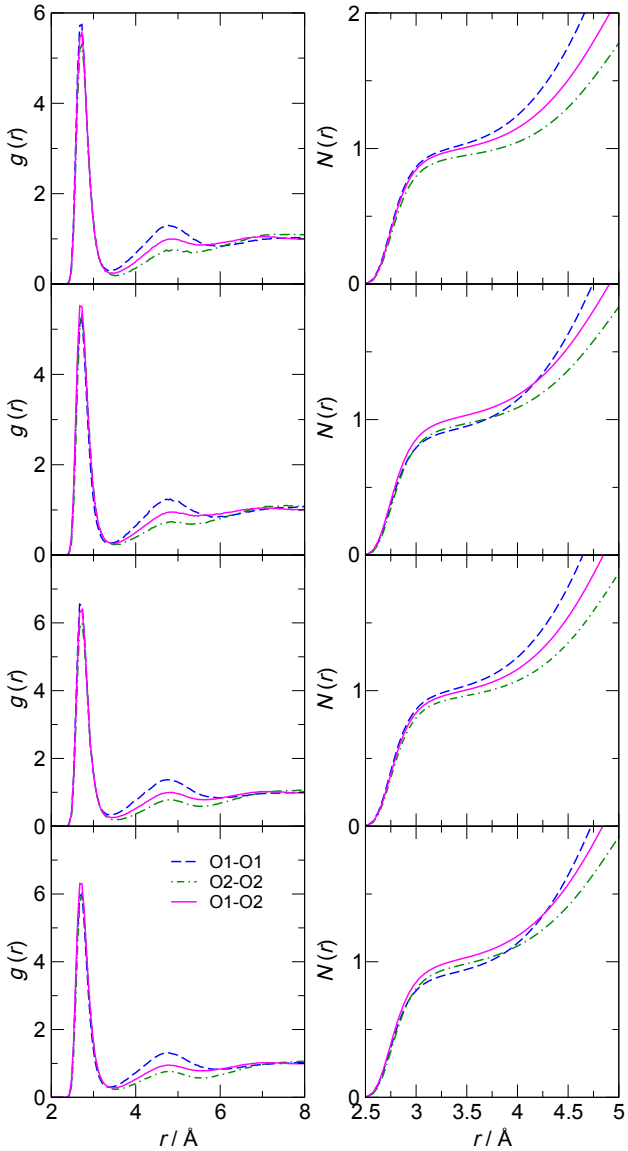

Figure 6: Primary primary, primary secondary, and secondary secondary O O radial distribution functions (left) and the corresponding number integrals (right) of equimolar MeOH/Pr2OH and MeOH/Bu2OH mixtures at 298.15 K and 1 bar. From top to bottom: MeOH/Pr2OH mixture with Pr2OH described by the TraPPE UA and M4 models, MeOH/Bu2OH mixture with Bu2OH described by the TraPPE UA and M4 models.

the secondary alcohols. The second peak is found at 4.8 A for all systems. While the rst and second peak positions are shared by all alcohols/models, there are subtle di erences in peak heights that are also re ected in the NIs. Due to the normalization of the RDFs (lower number densities of oxygen atoms for the MeOH/Bu2OH mixtures compared to the MeOH/Pr2OH mixtures), the rst peak is more intense for the MeOH/Bu2OH mixtures

than for the MeOH/Pr2OH mixtures. More important are the small changes in peak heights when comparing data for the TraPPE UA and M4 models. For the former, the most intense peak is found for the primary primary O O pair and the weakest peak for the secondary secondary O O pair as one might also infer from greater steric hindrance (or the larger LJ diameter for the CH group compared to the CH group). Interestingly, this inference does not hold when the secondary alcohol is represented by the M4 model. Here, the peak for the primary secondary O O pair is most intense, whereas those for primary primary and secondary-secondary O O pairs are similar in height.

The minimum in the RDFs at 3.5 A re ects the outer boundary of the rst shell of hydrogen-bonded neighbors, and the value of the NI at this distance (being an in ection point) gives the number of nearest neighbors in this shell. For these equimolar mixtures (or, more generally, for a mixture containing the same numbers of two di erent types of atoms), the NI for secondary O atoms surrounding a primary O atom (O1 O2 pair) is identical to that for primary O atoms surrounding a secondary O atom (O2 O1 pair). For the equimolar mixtures of the short-chain alcohols investigated here, the NI values at 3.5 A are close to 1; that is, each oxygen atom is in close proximity of two other oxygen atoms (e.g., the sum of O1 O1 and O1 O2 pairs or of O2 O2 and O2 O1 pairs). When Pr2OH and Bu2OH molecules are modelled by the TraPPE UA force eld, then the numbers of neareast neighbors are ordered as O1 O1 O1 O2 O2 O2, and the same order holds for the NIs for distances from 3 to 5 A. Although the TraPPE UA model yields endothermic mixing behavior with the magnitude of __ for the MeOH/Bu2OH mixture being about twice as large than for the MeOH/P2OH mixture, there is no sign in the NIs that points to the unlike O1 O2 contacts being disfavored. However, as expected from the exothermic mixing behavior observed when Pr2OH and Bu2OH are described by the M4 model, the numbers of nearest neighbors are slightly larger for the unlike O1 O2 pair. The NIs for the M4 model also exhibit crossing behavior. At short distances, the NI for the O1 O1 pair falls below that for the O2 O2 pair but, at about 3.7 A, the NI for the O1 O1 pair becomes larger than for

the O2 O2 pair. At about 4.2 A, the NI for the O1 O1 pair becomes also larger than that for the O1 O2 pair. The latter is connected to the second peak in the RDFs being always the highest for the O1 O1 pair. That is, the second-nearest neighbor packing e ciency is better for the hydroxyl groups of the smaller MeOH molecules.

Another way to quantify the structural di erences is the local composition enhancement (LCE), which is de ned as the ratio of the local to the bulk composition and can be calculated from the NIs. As shown in Fig. 7, representing the secondary alcohols by the M4 model (exothermic mixing behavior) results in an enrichment of about 5% for the unlike O2-O1 pair in the nearest neighbor shell, whereas it is depleted by a mere 1% for the TraPPE UA model (endothermic mixing behavior). The change of the model parameters appears to have only a minimal e ect for the O2 O2 pair. The depletion of surrounding oxygen atoms belonging to Pr2OH or Bu2OH molecules observed from about 4.2 A outwards is due to the higher packing e ciency of the MeOH molecules.

Given the strengths of hydrogen bonds, the mixing behavior also needs to be discussed in terms of changes in the number of hydrogen bonds and in the distribution of hydrogen-bonded aggregates. Of course, it needs to be recognized that there is no on o switch for a hydrogen bond, and that there is a continuum from strong to weak hydrogen bonds. Here we employ the approach suggested by Wernet that uses an elliptical boundary in terms of the O O distance and the O H O angle to decide on whether a pair of alcohol molecules is associated through a hydrogen bond. We nd that the elliptical boundary works particularly well for the alcohols investigated here (see Fig. 8).

Using heatmaps of the distribution of O O distances and O H O angles (also called radial angular distribution functions, Figs. 8 and S3 S14), we nd that placing the center of the elliptical boundary at = 2 75 A (i.e., near the rst peak in the O O RDFs) and at = 180° (i.e., a linear hydrogen bond) works well for all systems investigated here. This places the center of the ellipse in close proximity to the most intense spot in the heat map which signals the energetically most favorable arrangment of O O distance

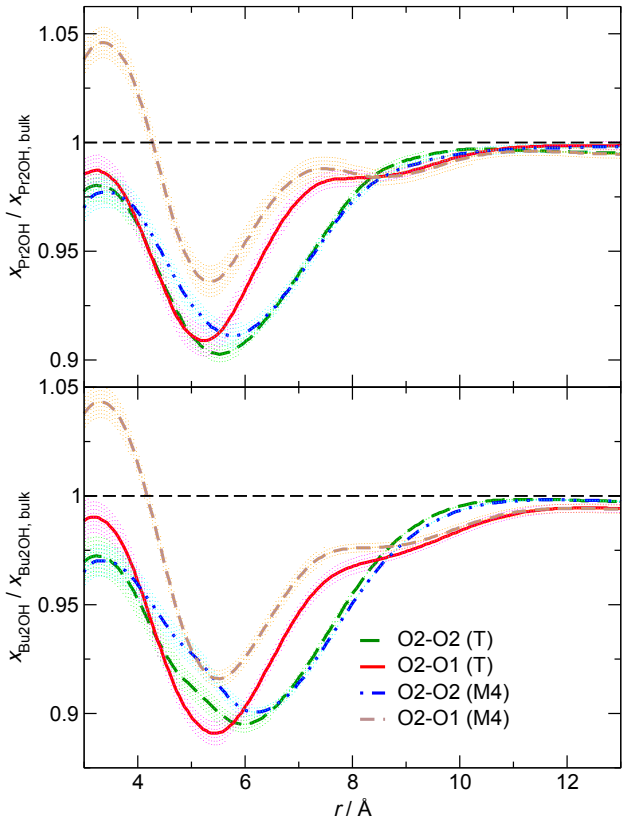

Figure 7: Local composition enhancement for equimolar MeOH/Pr2OH (top) and MeOH/Bu2OH (bottom) mixtures at 298.15 K and 1 bar. The curves with the secondary alcohol being the surrounding neighbors are shown for the TraPPE UA (T) and M4 models.

and O H O angle. The strictness of the hydrogen-bond criterion is controlled by the and parameters, where larger values lead to a more permissive criterion (i.e., including a larger fraction of weaker hydrogen bonds). It should be noted that the radial angular distribution functions are not symmetric (obviously, cannot be greater than 180°) because of the steeply repulsive potential at shorter separation; that is being more permissive on the shorter distance side causes a negligible overcounting of the number of strong or weak hydrogen (also considering the smaller volume elements at shorter distance). Here, two sets of parameters are utilized to examine the sensitivity of the hydrogen bond analysis with regard to the strictness of the hydrogen-bond criterion. The tighter criterion (= 0 55 A and = 35°) encompasses approximately the region where the radial-angular distribution value is larger than unity (see Fig. 8). The looser criterion (= 0 75 A and = 40°)

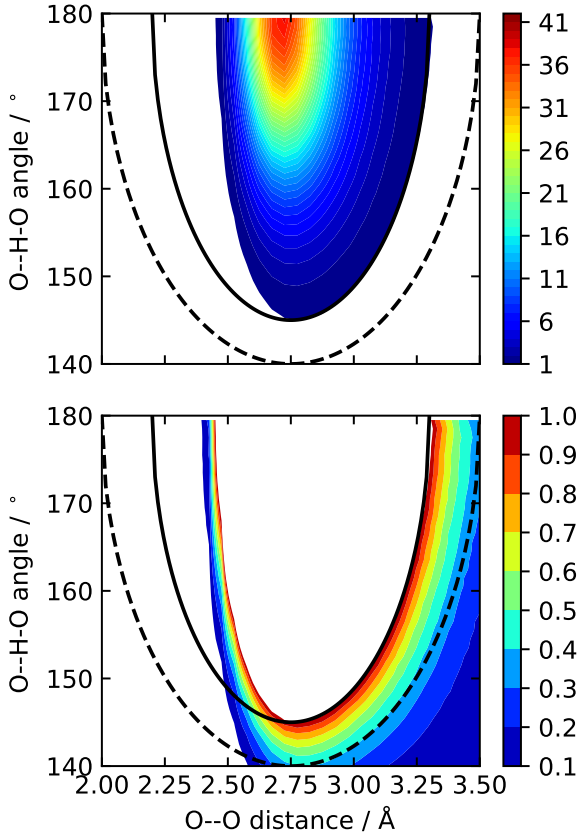

Figure 8: Heatmaps of the distribution of O O distances and O H O angles for Pr2OH molecules modelled with the M4 parameters in the neat liquid at 298.15 K and 1 bar. The solid and dashed boundaries indicate the tighter (= 0 55 A, = 35°) and looser (= 0 75 A, = 40°) criteria, respectively, forming ellipses centered at = 2 75 A and = 180°. The color scale in the top part highlights the region with the propensity being greater than that for a uniform distribution, and the bottom part highlights values below unity.

approximately encompasses the region where the radial-angular distribution value is larger than 0.5 (see Fig. 8). The precise boundary of these regions depends slightly on the alcohol and the force eld parameters. For example, using tighter distance (= 0 48 A) and looser angle (= 37°) parameters would better describe the region above unity for MeOH (Fig. S3) but, in the interest of generality, the analysis carried out here applies the same criterion for all systems.

The change in the hydrogen-bond number of mixing, , is de ned as the di erence between the number of hydrogen bonds per molecule for the real mixture, , and that

of the ideal mixture as follows

$$= \tag{12}$$

where is the mole fraction in the mixture and is the number of hydrogen bonds per molecule of type in its neat phase. The data reported in Tables 7 and S6 indicate that is smaller in magnitude than 0.004 for all mixtures, and the data for all mixtures fall almost within their combined 95% con dence levels. Although and values increase by 0 1 when switching from the tighter to the looser hydrogen-bond criterion, the values are not a ected by the choice of hydrogen-bond criterion. The values of 1.758 for Pr1OH and Bu1OH are slightly larger than the 1.753 observed for MeOH (all using the tighter criterion). The values for the secondary alcohols tend to be slightly lower than that for MeOH. Considering the e ect of switching from the TraPPE UA model to the M4 model, we observe a di erence between the two hydrogen-bond criteria. With the tighter criterion, values obtained with the M4 model are 0.005 larger than those for the TraPPE UA model. With the looser criterion, this di erence diminishes to 0.001. Despite that the M4 model yields a a negative enthalpy of mixing for MeOH with the secondary alcohols, the values are smaller than when the secondary alcohols are represented by the TraPPE UA model. That is the exothermic mixing behavior does not need to be associated with an increase in the number of hydrogen bonds.

Given a hydrogen-bond criterion (here the tighter criterion is used), the structure can further be analyzed in terms of the distribution of hydrogen-bonded aggregates. Fig. 9 presents the distribution of molecules over di erent aggregate sizes where is the fraction of molecules irrespective of molecule type that belongs to a certain cluster size, . Not shown here is the fraction of aggregates of a given size (i.e., normalized by the total number of aggregates instead of the total number of molecules) because is more relevant for the mixing behavior expressed in molar quantities. For all systems, the distributions show

Table 7: Number of hydrogen bonds per molecule in neat phases of PrOH and BuOH alcohols ( ), their equimolar binary mixtures with MeOH ( ), and the property change of mixing ( ) calculated with the tighter hydrogen-bond criterion. The value for MeOH in its neat phase is 1 7533 0 0013. The uncertainties ( ) are estimated at the 95% con dence levels.

systems		( )		( )		( )
Pr1OH	1.7584	0.0014	1.7560	0.0014	0.0001	0.0018
Pr2OH (T)	1.7403	0.0008	1.7464	0.0018	0 0004	0.0020
Pr2OH (M4)	1.7451	0.0007	1.7482	0.0021	0 0010	0.0023
Bu1OH	1.7583	0.0022	1.7554	0.0016	0 0005	0.0021
Bu2OH (T)	1.7510	0.0010	1.7499	0.0017	0 0022	0.0019
Bu2OH (M4)	1.7563	0.0010	1.7514	0.0024	0 0034	0.0025

a peak for = 4 or 5. For the neat liquids, the peak height increases from MeOH to primary alcohol to secondary alcohol represented by the TraPPE UA model to secondary alcohol represented by the M4 model due to the increasing steric hindrance. Similarly, the peaks are taller for neat BuOH than for neat PrOH systems. Switching from the TraPPE UA model to the M4 model also shifts the peak position downward from = 5 to 4.

These changes in the distribution over aggregate sizes o ers an explanation for the unusual exothermic mixing behavior observed for the mixtures of MeOH with (Pr2OH or Bu2OH). The preference for tetramer and pentamer aggregates is due to the formation of cyclic aggregates with hydrogen bonds, whereas linear or branched alcohol aggregates possess 1 hydrogen bonds. Thus, these cyclic aggregates are enthalpically favored because of the additional hydrogen bond, but the ring strain requires deviations from linearity which weakens the hydrogen bonds in tetramers and pentamers. The steric hindrance from the bulky branched alkyl groups makes it more di cult to form larger aggregates. For the neat liquids, the cumulative value passes through 0.5 (i.e., half of the molecules are found in smaller aggregates) at = 14 for MeOH, = 12 for Pr1OH and Bu1OH, = 11 for Pr2OH and Bu2OH represented by the TraPPE UA model, and = 9 for Pr2OH and Bu2OH represented by the M4 model. The values passing the 0.5 threshold calculated for the equimolar mixtures with (Pr1OH or Bu1OH) and with (Pr2OH or Bu2OH)

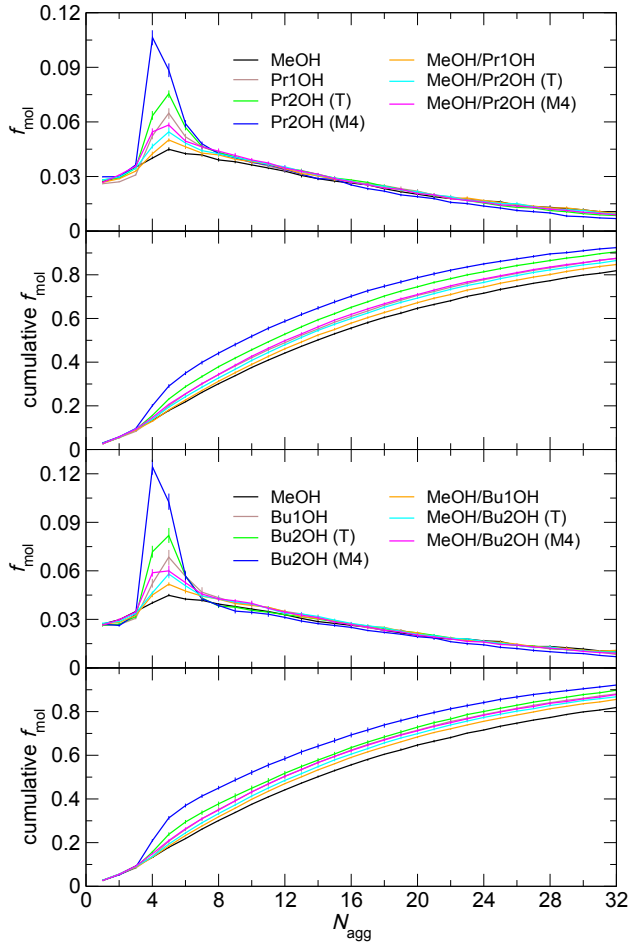

Figure 9: Fraction of molecules, , belonging to a hydrogen-bonded aggregate of size and the corresponding cumulative integral for neat phases and equimolar mixtures of MeOH and PrOH isomers (top parts) and MeOH and BuOH isomers (bottom parts) at 298.15 K and 1 bar. Data involving secondary alcohols are shown for the TraPPE UA (T) and M4 models. The error bars denote for the 95% con dence interval. The numerical data up to = 16 are provided in Tables S7 and S8.

represented by the TraPPE UA model are 13 and 12, respectively; that is, they coincide with or fall below the average for the two compounds in their neat phases. In contrast, the values passing the 0.5 threshold calculated for the equimolar mixtures with (Pr2OH or Bu2OH) represented by the M4 model are 12 in both cases exceeding the average of the neat systems. In fact, the cumulative curves for the MeOH/(Pr2OH or Bu2OH) mixtures with the M4 model are shifted to slightly larger values than for the TraPPE UA model. This is remarkable because the preferred aggregate size for secondary alcohols with the M4 model

is four, while it is ve for the TraPPE UA model. Thus, the preference for cross-association imbued by the M4 model (Figs. 6 and 7) diminishes the number of tetramer and pentamer aggregates and shifts the distribution of molecules to larger aggregates with less strain on their hydrogen bonds compared to the pure liquids and this, in turn, yields the exothermic mixing behavior.

The e ect of preferential solvation usually mitigates as temperature increases, indicating that the magnitude of the enthalpy of mixing may concommitantly decrease. To test the temperature dependence of the enthalpy of mixing, molecular simulations and COSMO-SAC calculations were also performed at a higher temperature (373.15 K) for mixtures of the PrOH and BuOH isomers with MeOH. The pressure for the molecular simulations was set at 5 bar to ensure that the systems remain in the liquid state, and only the M4 model for the secondary alcohols was investigated. One should be aware that the COSMO-SAC activity coe cients are pressure independent (i.e., assuming an incompressible liquid). For the mixtures of (Pr1OH or Bu1OH) with MeOH, both the molecular simulations and the experimental data show a downward shift in the positive __ at the higher temperature (see Fig. 10). On the other hand, the COSMO-SAC approach fails to capture the temperature dependence of the enthalpy of mixing. The partial derivative of ln with respect to temperature is small and not very sensitive to temperature. Based on Eq. 2, the increase in __ is simply dominated by the prefactor. Beyond the downward shift, both molecular simulation and experiment indicate a more signi cant skew to higher at the elevated temperature. This is due to the more facile disruption of the self-association for the larger species. The molar enthalpy of pure MeOH increases by 5.24 kJ/mol from 36 42 kJ/mol at 298.15 K to 31 18 kJ/mol at 373.15 K, whereas the molar enthalpy of pure Pr1OH increases by 8.26 kJ/mol from 37 45 kJ/mol at 298.15 K to 29 19 kJ/mol at 373.15 K.

The temperature e ect for the primary secondary alcohol mixtures is more signi cant

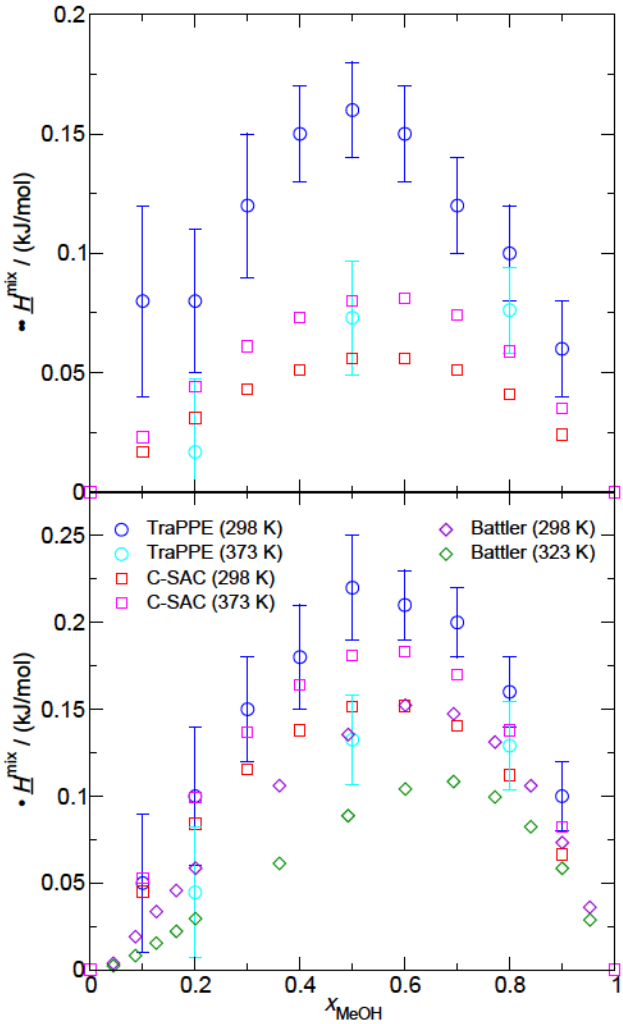

Figure 10: Comparison of the molar enthalpies of mixing for MeOH/Pr1OH (top) and MeOH/Bu1OH (bottom) binary mixtures at (373.15 K, 5 bar) and (298.15 K, 1 bar) predicted with the COSMO-SAC and TraPPE–UA models and measured experimentally at 323.15 and 298.15 K and 1 bar.[50] The numerical data at (373.15 K, 5 bar) are provided in Tables S9 and S10.

than for the primary–primary systems (compare Figs. 10 and 11) because it is even easier to disrupt self-aggregation of the secondary alcohols. The molar enthalpy of neat Pr2OH increases by 9.06 kJ/mol from −37.05 kJ/mol at 298.15 K to −27.99 kJ/mol at 373.15 K. Due to the stronger cross-association of the unlike species, the negative $\Delta\underline{H}^{\mathrm{mix}}$ becomes larger in magnitude, and the minimum in $\Delta\underline{H}^{\mathrm{mix}}$ does remain close to $x_{\mathrm{MeOH}} \approx 0.5$. We were not able to find experimental data at elevated temperature for the primary–secondary alcohol mixtures.

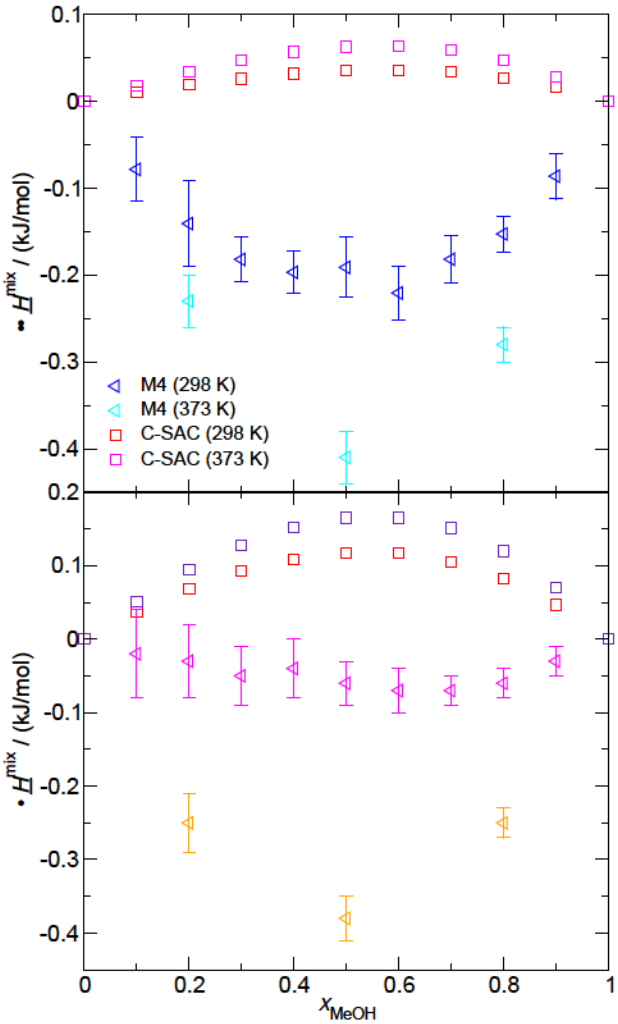

Figure 11: Comparison of the molar enthalpies of mixing for MeOH/Pr2OH (top) and MeOH/Bu2OH (bottom) binary mixtures at (373.15 K, 5 bar) and (298.15 K, 1 bar) predicted with the COSMO-SAC and TraPPE–UA models. The numerical data at (373.15 K, 5 bar) are provided in Tables S9 and S10.

A comparison of vapor–liquid equilibria for these alcohol mixtures is also informative. The vapor–liquid phase envelope can be constructed using the COSMO-SAC approach by ensuring that the fugacity (or chemical potential) of each component is identical in the two phases, i.e.,

$$y_i p = \gamma_i x_i p_i^{\mathrm{sat}} \tag{13}$$

where x_i and y_i are liquid and vapor compositions of species i, respectively. p_i^{sat} is the saturated pressure of component i. It should be noted that, for the COSMO-SAC predictions

presented here, the saturated vapor pressures of the pure compounds are determined based on experimental data and the Antoine equation, i.e., the activity coe cient model is only applied to predict the relative behavior as composition varies. In this case, therefore, it is unfair to directly compare the accuracy of the COSMO-SAC calculations to the force- eld-based Monte Carlo simulations where saturated vapor pressures and normal boiling points of the pure compounds must also be predicted and simulations for mixtures do not rely on experimental data for the pure compounds. Figs. 12 and 13 demonstrate the challenges of the fully predictive molecular simulations because the boiling points and the vapor pressures at the endpoints (neat states) deviate slightly from the corresponding experimental data. The small di erences at the endpoints cause a shift and/or expansion/compression for the phase envelopes. It should be noted that a shift (i.e., vapor pressures or boiling points for both compounds are over or under predicted to a similar extent) is less detrimental for the prediction of the separation factor than expansion/compression (i.e., predictions for the pure compounds deviate in opposite direction).

COSMO-SAC predicts a very accurate phase envelope for the MeOH/Bu1OH mixture (see Fig. 12), although the failure to capture the second-order change of the activity coe - cients with respect to temperature manifests itself in marginally larger deviations at 360 K. For the primary secondary alcohol mixtures that experimentally exhibit exothermic mixing, COSMO-SAC over predicts the vapor pressures in the pressure composition diagram for the MeOH/Pr2OH mixture at 323.15 K and under predicts the boiling point in the isobaric phase diagram for the MeOH/Bu2OH mixture at 1 atm (see Fig. 13). Here, the stronger cross-association leads to a lower vapor pressure and a higher boiling point.

The TraPPE UA model yields a slightly narrower phase envelope and under predicts the separation factor (ratio) for the MeOH/Bu1OH mixture (see Fig. 12) despite the correctly predicted endothermic mixing behavior because the normal boiling point of MeOH is slightly over predicted while that of Bu1OH is slightly under predicted. For the primary secondary alcohol mixtures, the M4 model yields shifted phase envelopes but very accurate

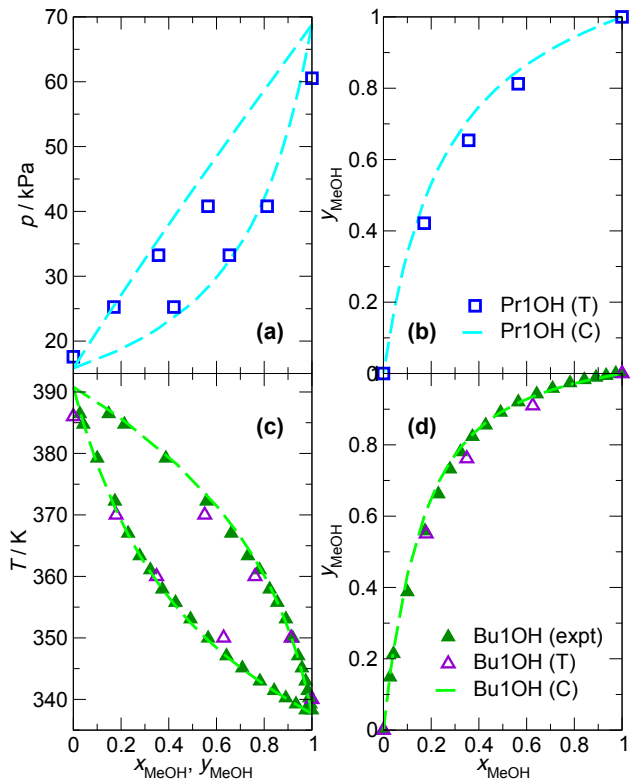

Figure 12: Pressure composition diagram (a) and separation factor (b) for the MeOH/Pr1OH mixture at = 328 15 K; temperature composition diagram (c) and separation factor (d) for the MeOH/Bu1OH mixture at = 1 bar. Data from molecular simulations with the TraPPE UA model (T, uncertainties are smaller than the symbol size), COSMO-SAC (C), and experimental measurements are shown. The numerical data are reported in Tables S11 and S12.

separation factors (see Fig. 13). In contrast, the TraPPE UA model yields compressed phase envelopes that fall closer to the experimental data for intermediate compositions, but separation factors that are under predicted. It is impossible to judge the relative contribution of the negative __ values observed for the M4 model to the more accurate prediction of the separation factor because the pure-phase vapor pressures of the secondary alcohols deviate in opposite directions for the M4 and TraPPE UA models.

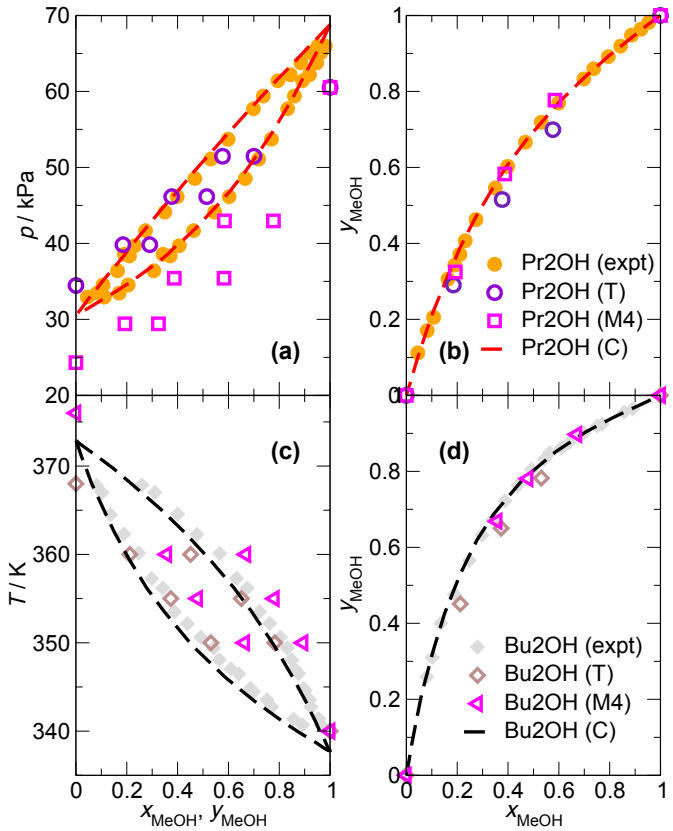

Figure 13: Pressure composition diagram (a) and separation factor (b) for the MeOH/Pr2OH mixture at = 328 15 K; temperature composition diagram (c) and separation factor (d) for the MeOH/Bu2OH mixture at = 1 bar. Data from molecular simulations with the TraPPE UA and M4 models (T and M4, uncertainties are smaller than the symbol size), COSMO-SAC (C), and experimental measurements are shown. The numerical data are reported in Tables S11 and S12.

Investigating mixtures of short-chain alcohols, we nd that molecular simulations with the TraPPE UA force eld and molecular modeling with the COSMO-SAC activity coe cient model predict endothermic mixing behavior for MeOH/(Pr1OH or Pr2OH or Bu1OH or Bu2OH) binary mixtures, whereas the experimental data yield exothermic mixing behavior for the primary secondary alcohol mixtures. To reproduce the exothermic mixing of primary secondary alcohols, the force eld parameters for the secondary alcohols were tuned by enhancing the partial charge on the O atom by 10% and the Lennard-Jones diameter of the -CH by 5% compared to the TraPPE UA force eld. Besides capturing the exothermic

mixing, the modi ed model also performs well for predicting liquid densities, vapor pressures at the experimental normal boiling points, and relative permitivities for Pr2OH and Bu2OH. The simulations with the TraPPE UA and M4 models yield a decrease in __ values as the temperature is increased for all four mixtures; a trend that agrees with the limited experimental data. In contrast, the COSMO-SAC approach yields the opposite trend.

A detailed analysis of the structures for the neat phases and the mixtures indicates only very minor changes between the TraPPE UA and the modi ed models and between mixtures with positive or negative enthalpy of mixing. This should not come as a surprise because the magnitude of __ for the MeOH/(Pr1OH or Pr2OH or Bu1OH or Bu2OH) binary mixtures is less than 0.2 kJ/mol. Considering that each alcohol molecule is involved in about two hydrogen bonds and that the strength of a hydrogen bond is about 15 kJ/mol, the __ values could be accounted for by a 1% change in the hydrogen-bond strength. Indeed we nd that the change in the number of hydrogen bonds upon mixing is negligible and even negative for the systems yielding exothermic mixing behavior (e.g., = 0 0034 0 0025 for the MeOH/Bu2OH mixture with the latter molecules represented by the modi ed model). On the other hand, the modi ed model yields slightly enhanced cross-association for the MeOH/(Pr2OH or Bu2OH) mixtures which results in a more signi cant shift from tetrameric to larger hydrogen-bonded aggregates than for the TraPPE UA model. Shifting the aggregate size distribution from cyclic tetramers and pentamers with strained hydrogen bonds to larger, less strained aggregates appears to be the underlying structural change associated with the exothermic mixing behavior of primary and secondary alcohols. Such a change in aggregation would not be re ected in the segmental surface charge distributions (-pro les).

Financial support from the National Science Foundation through the Chemical Measure-

ment & Imaging program with co-funding from the Interfacial Engineering program (Award CHE 2003246) is gratefully acknowledged. The computational resources for the molecular simulation were provided by the Minnesota Supercomputing Institute at the University of Minnesota and those for the COSMO-SAC calculations by the group of Shiang-Tai Lin at National Taiwan University. We thank Paul Mathias for bringing the unusual mixing behavior of the short-chain alcohols to our attention. CKC also thanks Jingyi Chen for insightful discussions on the elliptical HB criteria.

Tables providing the complete set of TraPPE UA force eld parameters for alcohols, numerical data for enthalpy and enthalpy of mixing obtained for the modi ed secondary alcohol models, numerical data for speci c densities, quantum-mechanical CM5 partial charges, and hydrogen-bond statistics with the looser criterion. Figures showing the -pro les of the alcohol molecules investigated here, dihedral angle distributions for Pr2OH, and heatmaps of the distribution of O O distances and O H O angles for additional neat phases and equimolar mixtures. Further details for the COSMO-SAC alcohol model and simulation details for the calculation of vapor pressure and relative permitivity.

(1) Jiang, X.; Wang, Y.; Li, M. Selecting Water-alcohol Mixed Solvent for Synthesis of Polydopamine Nano-spheres Using Solubility Parameter. , , 6070.

(2) Ribeiro, M. M.; Neumann, V. A.; Padoveze, M. C.; Graziano, K. U. E cacy and E ectiveness of Alcohol in the Disinfection of Semi-critical Materials: A Systematic Review. , , 741 752.

(3) Ali, O. M.; Abdullah, N. R.; Mamat, R.; Abdullah, A. A. Comparison of the E ect of Di erent Alcohol Additives with Blended Fuel on Cyclic Variation in Diesel Engine. , , 2357 2362.

(4) Ra erty, J. L.; Siepmann, J. I.; Schure, M. R. Mobile Phase e ects in Reversed-Phase Liquid Chromatography: A Comparison of Acetonitrile/Water and Methanol/Water Solvents as Studied by Molecular Simulation. , , 2203 2213.

(5) Guiochon, G.; Tarafder, A. Fundamental Challenges and Opportunities for Preparative Supercritical Fluid Chromatography. , , 1037 1114.

(6) Rosales-Calderon, O.; Arantes, V. A Review on Commercial-scale High-value Products that Can be Produced Alongside Cellulosic Ethanol. , , 240.

(7) Brunetti, A.; Migliori, M.; Cozza, D.; Catizzone, E.; Giordano, G.; Barbieri, G. Methanol Conversion to Dimethyl Ether in Catalytic Zeolite Membrane Reactors. , , 10471 10479.

(8) Bogorad, I. W.; Chen, C.-T.; Theisen, M. K.; Wu, T.-Y.; Schlenz, A. R.; Lam, A. T.; Liao, J. C. Building Carbon carbon Bonds Using a Biocatalytic Methanol Condensation Cycle. , , 15928 15933.

(9) Qi, J.; Finzel, J.; Robatjazi, H.; Xu, M.; Ho man, A. S.; Bare, S. R.; Pan, X.; Christopher, P. Selective Methanol Carbonylation to Acetic Acid on Heterogeneous Atomically Dispersed ReO /SiO Catalysts. , , 14178 14189.

(10) Brown, M.; Parkyns, N. Progress in the Partial Oxidation of Methane to Methanol and Formaldehyde. , , 305 335.

(11) Waters, T.; O Hair, R. A.; Wedd, A. G. Catalytic Gas Phase Oxidation of Methanol to Formaldehyde. , , 3384 3396.

(12) Barton, E. E.; Rampulla, D. M.; Bocarsly, A. B. Selective Solar-driven Reduction of CO to Methanol Using a Catalyzed p-GaP Based Photoelectrochemical Cell. , , 6342 6344.

(13) Menard, G.; Stephan, D. W. Room Temperature Reduction of CO to Methanol by Al-Based Frustrated Lewis Pairs and Ammonia Borane. , , 1796 1797.

(14) Hu , C. A.; Sanford, M. S. Cascade Catalysis for the Homogeneous Hydrogenation of CO to Methanol. , , 18122 18125.

(15) Kim, S.; Yoon, C.; Ham, S.; Park, J.; Kwon, O.; Park, D.; Choi, S.; Kim, S.; Ha, K.; Kim, W. Chemical Use in the Semiconductor Manufacturing Industry. , , 109 118.

(16) Swana, J.; Yang, Y.; Behnam, M.; Thomson, R. An Analysis of Net Energy Production and Feedstock Availability for Biobutanol and Bioethanol. , , 2112 2117.

(17) Renon, H.; Prausnitz, J. M. Local Compositions in Thermodynamic Excess Functions for Liquid Mixtures. , , 135 144.

(18) Abrams, D. S.; Prausnitz, J. M. Statistical Thermodynamics of Liquid Mixtures: A New Expression for the Excess Gibbs Energy of Partly or Completely Miscible Systems. , , 116 128.

(19) Fredenslund, A.; Jones, R. L.; Prausnitz, J. M. Group-contribution Estimation of Activity Coe cients in Nonideal Liquid Mixtures. , , 1086 1099.

(20) Klamt, A. Conductor-like Screening Model for Real Solvents: A New Approach to the Quantitative Calculation of Solvation Phenomena. , , 2224 2235.

(21) Lin, S.-T.; Sandler, S. I. A Priori Phase Equilibrium Prediction from a Segment Contribution Solvation Model. , , 899 913.

(22) Chapman, W. G.; Gubbins, K. E.; Jackson, G.; Radosz, M. SAFT Equation-of-state Solution Model for Associating Fluids. , , 31 38.

(23) Gross, J.; Sadowski, G. Perturbed-chain SAFT: An Equation of State Based on a Perturbation Theory for Chain Molecules. , , 1244 1260.

(24) McCabe, C.; Kiselev, S. B. Application of Crossover Theory to the SAFT-VR Equation of State: SAFT VRX for Pure Fluids. , , 2839 2851.

(25) La tte, T.; Apostolakou, A.; Avendano, C.; Galindo, A.; Adjiman, C. S.; A., M. E.; Jackson, G. Accurate Statistical Associating Fluid Theory for Chain Molecules formed from Mie Segments. , , 154504.

(26) McDonald, I. R. -Ensemble Monte Carlo Calculations for Binary Liquid Mixtures. , , 41 58.

(27) Panagiotopoulos, A.; Quirke, N.; Stapleton, M.; Tildesley, D. Phase Equilibria by Simulation in the Gibbs Ensemble Alternative derivation, generalization and application to mixture and membrane equilibria. , , 527 545.

(28) Mathias, P. M. 110th Anniversary: A Case Study on Developing Accurate and Reliable Excess Gibbs Energy Correlations for Industrial Application. , , 12465 12477.

(29) Polak, J.; Murakami, S.; Lam, V. T.; P ug, H. D.; Benson, G. C. Molar Excess Enthalpies, Volumes, and Gibbs Free Energies of Methanol Isomeric Butanol Systems at 25 °C. , , 2457 2465.

(30) Murakami, S.; Benson, G. Thermodynamic Properties of Some Isomeric Butyl Alcohol Mixtures. , , 74 79.

(31) Chen, B.; Poto , J. J.; Siepmann, J. I. Monte Carlo Calculations for Alcohols and Their Mixtures with Alkanes. Transferable Potentials for Phase Equilibria. 5. United-Atom Description of Primary, Secondary, and Tertiary Alcohols. , , 3093 3104.

(32) Hsieh, C.-M.; Sandler, S. I.; Lin, S.-T. Improvements of COSMO-SAC for Vapor Liquid and Liquid Liquid Equilibrium Predictions. , , 90 97.

(33) Chang, C.-K.; Chen, W.-L.; Wu, D. T.; Lin, S.-T. Improved Directional Hydrogen Bonding Interactions for the Prediction of Activity Coe cients with COSMO-SAC. , , 11229 11238.

(34) Lorentz, H. A. Ueber die Anwendung des Satzes vom Virial in der kinetischen Theorie der Gase. , , 127 136.

(35) Allen, M.; Tildesley, D. ; Clarendon Press, Oxford, 1989.

(36) Siepmann, J. I.; Martin, M. G.; Chen, B.; Wick, C. D.; Stubbs, J. M.; Poto , J. J.; Eggimann, B. L.; McGrath, M. J.; Zhao, X. S.; Anderson, K. E.; Ra erty, J. L.; Rai, N.; Maerzke, K. A.; Keasler, S. J.; Bai, P.; Fetisov, E. O.; Shah, M. S.; Chen, Q. P.;

DeJaco, R. F.; Chen, J. L.; Bai, X.; Sun, Y.-Z.-S.; Chang, C.-K. Monte Carlo for Complex Chemical Systems Minnesota, V21.4. 2021.

(37) Martin, M. G.; Siepmann, J. I. Novel Con gurational-Bias Monte Carlo Method for Branched Molecules. Transferable Potentials for Phase Equilibria. 2. United-Atom Description of Branched Alkanes. , , 4508 4517.

(38) Staverman, A. J. The Entropy of High Polymer Solutions - Generation of Formulae. , , 163 174.

(39) Chen, W.-L.; Lin, S.-T. Explicit Consideration of Spatial Hydrogen Bonding Direction for Activity Coe cient Prediction Based on Implicit Solvation Calculations. , , 20367 20376.

(40) Chang, C.-K.; Lin, S.-T. Improved Prediction of Phase Behaviors of Ionic Liquid Solutions with the Consideration of Directional Hydrogen Bonding Interactions. , , 3550 3559.

(41) te Velde, G.; Bickelhaupt, F. M.; Baerends, E. J.; Fonseca Guerra, C.; van Gisbergen, S. J. A.; Snijders, J. G.; Ziegler, T. Chemistry with ADF. , , 931 967.

(42) Pye, C. C.; Ziegler, T. An Implementation of the Conductor-like Screening Model of Solvation within the Amsterdam Density Functional Package. , , 396 408.

(43) Baerends, E. J.; Ziegler, T.; Atkins, A. J.; Autschbach, J.; Bashford, D.; Baseggio, O.; Berces, A.; Bickelhaupt, F. M.; Bo, C.; Boerritger, P. M.; Cavallo, L.; Daul, C.; Chong, D. P.; Chulhai, D. V.; Deng, L.; Dickson, R. M.; Dieterich, J. M.; Ellis, D. E.; van Faassen, M.; Ghysels, A.; Giammona, A.; van Gisbergen, S. J. A.; Goez, A.; Gotz, A. W.; Gusarov, S.; Harris, F. E.; van den Hoek, P.; Hu, Z.; Jacob, C. R.;

Jacobsen, H.; Jensen, L.; Joubert, L.; Kaminski, J. W.; van Kessel, G.; Konig, C.; Kootstra, F.; Kovalenko, A.; Krykunov, M.; van Lenthe, E.; McCormack, D. A.; Michalak, A.; Mitoraj, M.; Morton, S. M.; Neugebauer, J.; Nicu, V. P.; Noodleman, L.; Osinga, V. P.; Patchkovskii, S.; Pavanello, M.; Peeples, C. A.; Philipsen, P. H. T.; Post, D.; Pye, C. C.; Ramanantoanina, H.; Ramos, P.; Ravenek, W.; Rodr guez, J. I.; Ros, P.; Ruger, R.; Schipper, P. R. T.; Schluns, D.; van Schoot, H.; Schreckenbach, G.; Seldenthuis, J. S.; Seth, M.; Snijders, J. G.; Sola, M.; M., S.; Swart, M.; Swerhone, D.; te Velde, G.; Tognetti, V.; Vernooijs, P.; Versluis, L.; Visscher, L.; Visser, O.; Wang, F.; Wesolowski, T. A.; van Wezenbeek, E. M.; Wiesenekker, G.; Wol , S. K.; Woo, T. K.; Yakovlev, A. L. ADF2017, SCM, Theoretical Chemistry, Vrije Universiteit, Amsterdam, The Netherlands, https://www.scm.com. 2017.

(44) Becke, A. D. Density-Functional Exchange-Energy Approximation with Correct Asymptotic Behavior. , , 3098 3100.

(45) Perdew, J. P. Density-Functional Approximation for the Correlation Energy of the Inhomogeneous Electron Gas. , , 8822 8824.

(46) P ug, H. D.; Pope, A. E.; Benson, G. C. Heats of Mixing of Normal Alcohols at 25°C. , , 408 410.

(47) Khurma, J. R.; Fenby, D. V. Thermochemical Study of Deuterium Exchange Reactions in Water-Alcohol and Alcohol-Alcohol Systems. , , 2443 2447.

(48) Pope, A. E.; P ug, H. D.; Dacre, B.; Benson, G. C. Molar Excess Enthalpies of Binary n-Alcohol Systems at 25°C. , , 2665 2674.

(49) Diaz-Pena, M.; Pernandez-Martin, F. Calor de Mezcla del Distema n-Butanol + Metanol at 25.0°C. , , 323 330.

(50) Battler, J. R.; Rowley, R. L. Excess Enthalpies between 293 and 323 K for Constituent

Binaries of Ternary Mixtures Exhibiting Partial Miscibility.
, , 719 732.

(51) Nan, Y.; Hou, Y.; Yu, Q. Measurement of Excess Molar Enthalpies of Some Alkan-1-ol/Iso-Propanol Binary Systems. , , 105.

(52) Haase, R.; Tillmann, W. Mixing Properties of the Liquid Systems Methanol + 2-Propanol and 1-Propanol + 2-Propanol. , , 121 131.

(53) Kumagai, A.; Yokoyama, C. Liquid Viscosity of Binary Mixtures of Methanol with Ethanol and 1-Propanol from 273.15 to 333.15 K. , , 3 13.

(54) Wei, I. C.; Rowley, R. L. Binary Liquid Mixture Viscosities and Densities.
, , 332 335.

(55) Khan, W. G.; Ha z ur, R.; Siddique, S.; Ansari, M. S. Density and Excess Molar Volumes of 1-Butanol + Methanol + Electrolyte Systems in the Temperature Range 293.15 308.15 K. , , 1368 1377.

(56) Marenich, A. V.; Jerome, S. V.; Cramer, C. J.; Truhlar, D. G. Charge Model 5: An Extension of Hirshfeld Population Analysis for the Accurate Description of Molecular Interactions in Gaseous and Condensed Phases. , ,
527 541.

(57) M ller, C.; Plesset, M. S. Note on an Approximation Treatment for Many-Electron Systems. , , 618 622.

(58) Frisch, M. J.; Trucks, G. W.; Schlegel, H. B.; Scuseria, G. E.; Robb, M. A.; Cheeseman, J. R.; Scalmani, G.; Barone, V.; Petersson, G. A.; Nakatsuji, H.; Li, X.; Caricato, M.; Marenich, A. V.; Bloino, J.; Janesko, B. G.; Gomperts, R.; Mennucci, B.; Hratchian, H. P.; Ortiz, J. V.; Izmaylov, A. F.; Sonnenberg, J. L.; Williams-Young, D.; Ding, F.; Lipparini, F.; Egidi, F.; Goings, J.; Peng, B.; Petrone, A.; Hender-

son, T.; Ranasinghe, D.; Zakrzewski, V. G.; Gao, J.; Rega, N.; Zheng, G.; Liang, W.; Hada, M.; Ehara, M.; Toyota, K.; Fukuda, R.; Hasegawa, J.; Ishida, M.; Nakajima, T.; Honda, Y.; Kitao, O.; Nakai, H.; Vreven, T.; Throssell, K.; Montgomery, J. A., Jr.; Peralta, J. E.; Ogliaro, F.; Bearpark, M. J.; Heyd, J. J.; Brothers, E. N.; Kudin, K. N.; Staroverov, V. N.; Keith, T. A.; Kobayashi, R.; Normand, J.; Raghavachari, K.; Rendell, A. P.; Burant, J. C.; Iyengar, S. S.; Tomasi, J.; Cossi, M.; Millam, J. M.; Klene, M.; Adamo, C.; Cammi, R.; Ochterski, J. W.; Martin, R. L.; Morokuma, K.; Farkas, O.; Foresman, J. B.; Fox, D. J. Gaussian 16 Revision C.01. 2016; Gaussian Inc. Wallingford CT.

(59) Smith, B. D.; Srivastava, R. ; Elsevier: Amsterdam, 1986.

(60) Haynes, W. ; CRC Press, 2009.

(61) Nunez-Rojas, E.; Aguilar-Pineda, J. A.; Perez de la Luz, A.; de Jesus Gonzalez, E. N.; Alejandre, J. Force Field Benchmark of the TraPPE UA for Polar Liquids: Density, Heat of Vaporization, Dielectric Constant, Surface Tension, Volumetric Expansion Co- e cient, and Isothermal Compressibility. , , 1669 1678.

(62) Humphrey, W.; Dalke, A.; Schulten, K. VMD: Visual Molecular Dynamics. , , 33 38.

(63) Wernet, P.; Nordlund, D.; Bergmann, U.; Cavalleri, M.; Odelius, M.; Ogasawara, H.; Naslund, L. A.; Hirsch, T. K.; Ojamae, L.; Glatzel, P.; Pettersson, L. G. M.; Nilsson, A. The Structure of the First Coordination Shell in Liquid Water. , , 995 999.

(64) Stubbs, J. M.; Siepmann, J. I. Aggregation in Dilute Solutions of 1-Hexanol in n-Hexane: A Monte Carlo Simulation Study. , , 3968 3978.

(65) Stubbs, J. M.; Siepmann, J. I. Elucidating the Vibrational Spectra of Hydrogen-Bonded Aggregates in Solution: Electronic Structure Calculations with Implicit Solvent and First-Principles Molecular Dynamics Simulations with Explicit Solvent for 1-Hexanol in n-Hexane. , , 4722 4729.

(66) Ploetz, E. A.; Bentenitis, N.; Smith, P. E. Developing force elds from the microscopic structure of solutions. , , 43 47.

(67) Arce, A.; Mart nez-Ageitos, J.; Rodil, E.; Soto, A. Phase equilibria involved in extractive distillation of 2-methoxy-2-methylpropane+methanol using 1-butanol as entrainer. , , 207 218.

(68) Freshwater, D. C.; Pike, K. A. Vapor-liquid equilibrium data for systems of acetone-methanol-isopropanol. , , 179 183.

(69) Man, X.; Jiao, T.; Wang, Z.; Zhang, X.; Zhang, X. Isobaric Vapor Liquid Equilibrium Measurements and Separation Process for the Quinary Methanol + Methylal + 2-Butanol + 2-(Methoxymethoxy)-butane + ( )-Di-sec-butoxymethane System. , , 5038 5048.

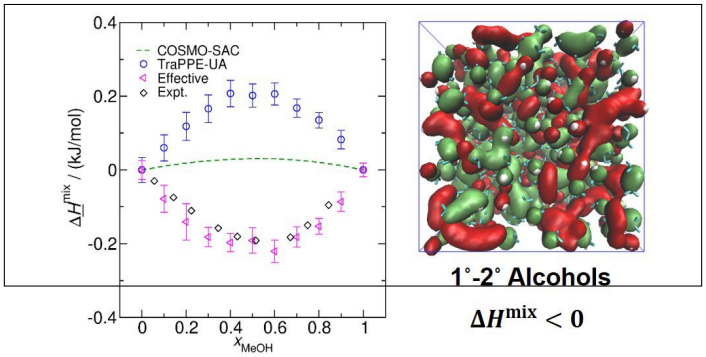
COSMO-SAC
TraPPE-UA
Effective
Expt.
ΔH^{mix} / (kJ/mol)
x_{MeOH}
0.4
0.2
0
-0.2
-0.4
0
0.2
0.4
0.6
0.8
1
1°-2° Alcohols
$\Delta H^{mix} < 0$